ADVANCED MATERIALS INTERFACES
www.advmatinterfaces.de

Green and Fire Resistant Nanocellulose/Hemicellulose/Clay Foams

Federico Carosio, Lilian Medina, Joby Kochumalayil, and Lars A. Berglund*

Lightweight polymer foams from synthetic polymers are commonly used in a wide-spread spectrum of application fields. Their intrinsic flammability coupled with restrictions on flame retardant chemicals poses a severe threat to safety. Here, fire resistant foams comprising biobased components capable of replacing petroleum-based foams are investigated. Cellulose nanofibers are combined with 2D montmorillonite nanoplatelets and a native xyloglucan hemicellulose binder, using a water-based freeze casting approach. Due to the silicate nanoplatelets, these lightweight foams self-extinguish the flame during flammability tests. The limiting oxygen index is as high as 31.5% and in the same range as the best fire-retardant synthetic foams available. In cone calorimetry, the foams display extremely low combustion rates. Smoke release is near the detection limit of the instrument. In addition, the foams are withstanding the penetration of a flame torch focused on one side of the specimen (*T* on surface 800 °C) and structural integrity is maintained. At the same time, the unexposed side is insulated, as demonstrated by a through-thickness temperature drop of 680 °C cm^{-1}. The results represent a tremendous opportunity for the development of fire-safe foams combining excellent sustainability with multifunctional performance.

1. Introduction

Foamed polymers represent a wide class of materials widely employed in packaging, cushioning and insulation applications. Indeed, low densities coupled with acoustic and/or heat transfer insulation explain the widespread use of these materials in civil, residential and industrial buildings. Unfortunately, while the application of polymer foams provides advantages in building energy efficiency, noise reduction and as load-bearing sandwich core materials, their organic nature poses severe risks to safety for fire start or propagation.[1,2] In addition, toxicological and environmental concerns for flame retardant chemicals recently resulted in the reduction or removal of such chemicals from polymer formulations, thus increasing the risk of fire as shown in recent tragic events.[3–5] In order to solve this problem, novel nanotechnology-based approaches to fire safety are under development.[6–9] Within this context, the use of green and sustainable materials is also desirable and has been proven to provide promising results while being in accordance with a circular economy where renewable resources are valorized.[10–12] In particular, water-based processing of biological polymers in combination with nanoparticles is a viable strategy for coatings or bulk materials with improved flame retardant characteristics.[13–15] For instance, layer by layer assembled nanostructured coatings from chitosan, alginates and platelet-like nanoparticles can impart flame retardant characteristics to open cell foams for cushioning or acoustic insulation applications.[16–20] Freeze casting of stable colloidal suspensions can be exploited for rigid foams with peculiar internal structure and unique composition.[21,22] The process involves freezing the suspension and then removing the ice crystals by sublimation. The pores structure results from removal of the ice phase. The foams normally contain alginates or nanocellulose and a large volume fraction of inorganic nanoparticles such as layered double hydroxide, sodium montmorillonite, kaolin and sepiolite.[21,23–25] Cellulose nanofibrils (CNF) can be used to form a continuous matrix in the cell wall of the foams. High-strength fibrils having dimensions of 4–10 nm in diameter and 0.7–2 µm in length can be conveniently disintegrated from wood and represent one of the most promising nano-building block for the production of advanced materials.[26] The freeze casting of CNF/nanoparticles hydrocolloids yields rigid foams where nano-structuration of the cell wall occurs naturally during ice crystal formation and growth.[27] This approach allows for higher inorganic nanoparticle concentration than in "conventional" polymer nanocomposite foams. The nanoparticles can provide substantial FR properties since the release of volatiles is hindered and heat shielding is provided.

F. Carosio
Dipartimento di Scienza Applicata e Tecnologia
Politecnico di Torino
Alessandria Campus
Viale Teresa Michel 5, Alessandria 15121, Italy
E-mail: federico.carosio@polito.it
L. Medina, J. Kochumalayil, L. A. Berglund
Wallenberg Wood Science Center
Department of Fiber and Polymer Technology
Royal Institute of Technology
Stockholm SE-10044, Sweden

The ORCID identification number(s) for the author(s) of this article can be found under https://doi.org/10.1002/admi.202101111.

DOI: 10.1002/admi.202101111

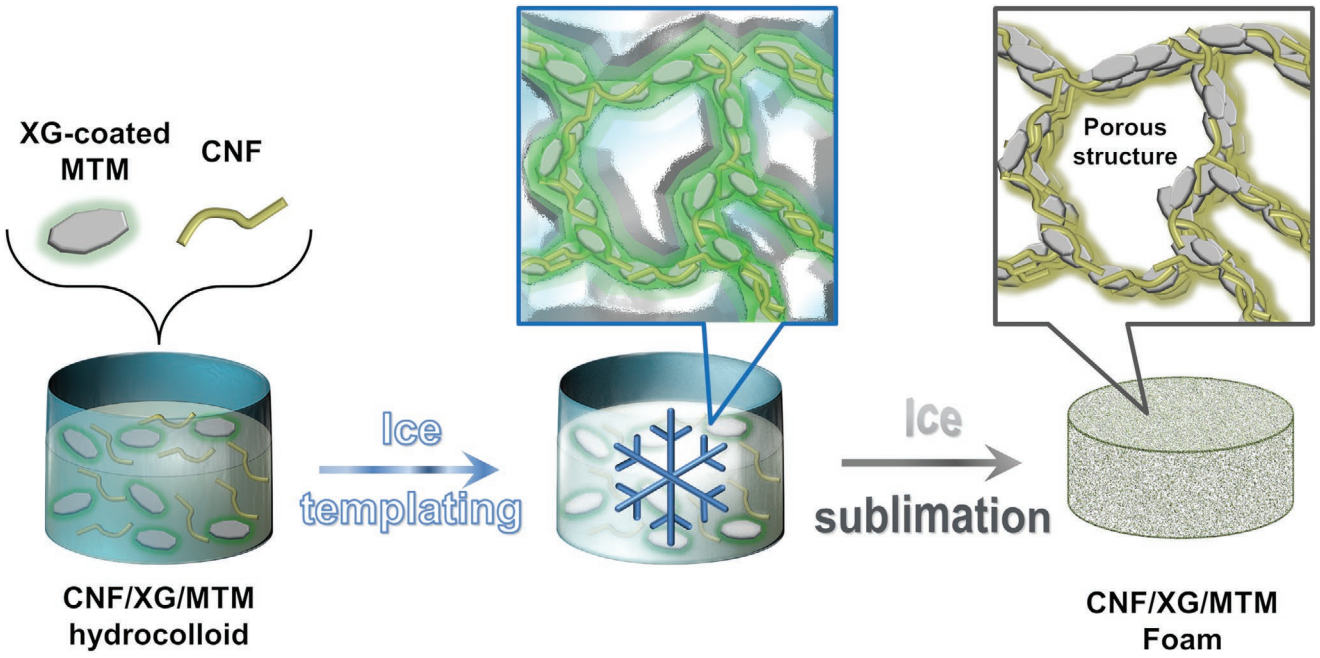

Figure 1. Schematization of the procedure adopted for the preparation of the CNF/XG/MTM foam.

For freeze casting, CNF/clay interfacial interactions may be non-ideal, and a third component polymer binder (e.g., polyvinyl alcohol, PVA) can improve mechanical properties to become comparable with or superior to state of the art materials.[28] The use of PVA limits the sustainability of the foams and reduces flame protection. Indeed, a synthetic polymer phase not only adds flammable organic components also limits CNF-nanoparticle interactions deemed responsible for flame retardancy in CNF/clay materials.[29,30] Here, we use a biological polysaccharide as a third component providing favorable mechanical properties to the CNF/clay foam (Table S2, Supporting Information), without compromising fire safety. To this aim, xyloglucan (XG)[31] is adsorbed on the surface of montmorillonite clay (MTM) platelets and then mixed with CNF in order to produce green and fire-proofed foams of 98.5% porosity by freeze casting (**Figure 1**). The composition is CNF/XG/MTM 27/40/33 wt%.

Xyloglucan is a polysaccharide classified as a hemicellulose and found in the primary cell walls in plants, for instance in parenchyma cells of fruits and vegetables. The main chain is identical to cellulose, but has heterogeneously positioned side-group substitutions, so that the solid polymer is amorphous. In the plant cell wall structure, XG molecules are linking cellulose fibrils,[32,33] which is the main biological role of all hemicelluloses, so that plant cell wall properties can be controlled. XG thus adsorbs strongly to cellulose. In addition, xyloglucan provides good interactions with montmorillonite clay in the presence of monovalent ions (e.g., Na^+). High-strength and surprisingly humidity-resistant nanocomposite films can be prepared, where XG is a continuous matrix reinforced by MTM clay.[34,35] High molar mass XG is thus a good candidate for green, ternary CNF-clay foams.

Nanostructured cell walls are formed during preparation of high-porosity (98.5%) foams and have so-called brick and mortar nanocomposite cell wall structure. The foams show high flame retardancy: low combustion rates and self-extinguishing behaviour during flammability tests. In addition, the foams could withstand a flame torch (*T* on the exposed surface close to 800 °C), maintaining structural integrity and successfully insulating the unexposed side of the foam. The results suggest an opportunity for fire-safe foams where sustainability and performance are combined.

2. Results and Discussion

2.1. Morphology

The morphology of foams was evaluated by FESEM. **Figure 2** presents the micrographs.

The CNF/XG/MTM foams show porous cellular structures (scale bar 40 µm) of high-porosity foams produced by isotropic ice templating.[28] The structure is not of the type in open cell foams, but rather a mixture of closed "spherical" cells and irregular, closed cells of various size and geometry. The composition is CNF/XG/MTM 27/40/33 wt%, the density of 0.029 g cm^{-3}, and the porosity of 98.5% (Table S1, Supporting Information). The cell walls are extremely thin with thicknesses below 1 µm. Elemental mapping performed on the foam cross-section clearly show a homogeneous distribution of MTM main elements (Figure S1, Supporting Information). High magnification micrographs, performed on the cell wall cross-section (Figure 2a) show the formation of a layered structure often referred to as "brick and mortar," where XG-coated MTM nanoplatelets (bricks) are embedded within a continuouos CNF matrix (mortar). Note that CNF is unlikely to be a separate phase from XG but rather partially intermixed, since the XG coating of MTM is water-swollen during the process. The resulting, possible, structure is illustrated in Figure 2b. During ice-formation, ice crystals are nucleated and CNF and XG/MMT

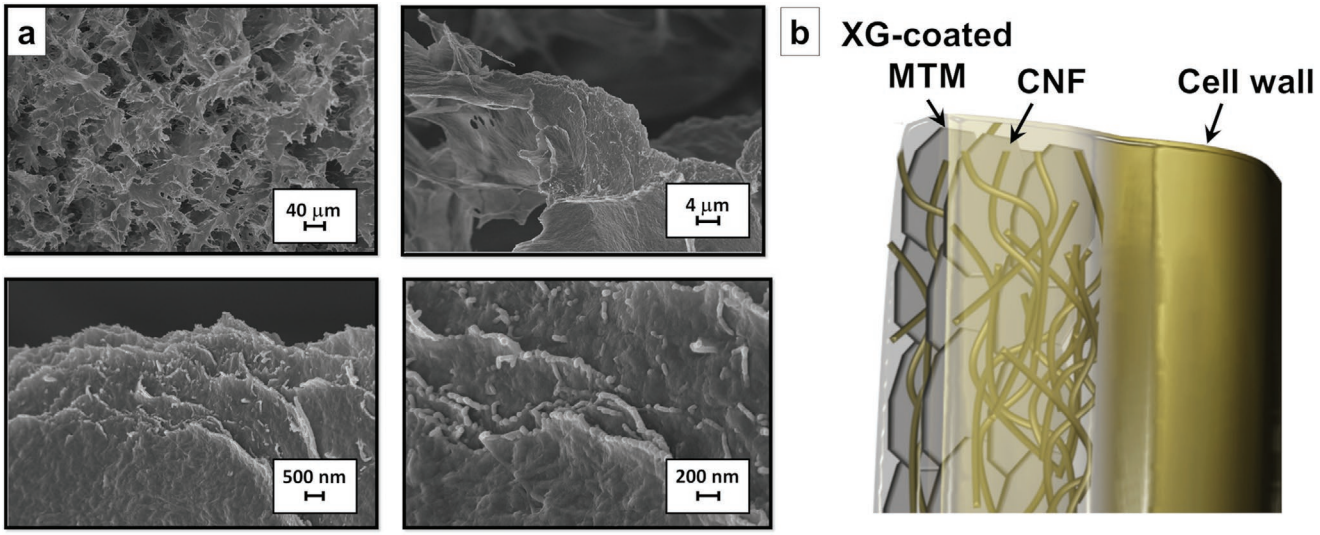

Figure 2. FESEM images at different magnifications of a) freeze-fractured foam structures (98.5 porosity) and b) sketch of the proposed cell wall structure. Note that the cell wall has a matrix in the form of CNF, where XG-coated MTM platelets are distributed as platelet reinforcement.

components are pushed to form interstitial regions, which form cell walls after ice phase sublimation. The mechanical properties of the prepared foams are similar to comparable ternary systems where strengthening binders such as PVA or cross-linkers such as boric acid and glutaraldehyde have been used to improve strength of CNF-based foams (Table S2, Supporting Information). XG acts as binder between MTM and CNF due to favorable interactions with both components former.[31,34,35] It is worth mentioning that a foam prepared from only CNF and MTM would result in inferior mechanical properties which would limit its practical application.

2.2. Flame Retardant Characterization

The flame retardant properties were evaluated by flammability tests in horizontal configuration, limiting oxygen index (LOI) and cone calorimetry. This provides a complementary set of information about the propensity of a material to start or propagate a fire. Flammability and LOI evaluate the response to a small flame mimicking one of the most common sources of ignition during a fire. Cone calorimetry evaluates the response to an impinging heat flux typical of a developing fire in its early stages.[36] **Figure 3** collects snapshots during flammability tests, LOI values of rigid foams from the literature, cone calorimetry heat release rate HRR and smoke production rate SPR plots along with integral values and a comparison of cone calorimetry parameters. A commercially available rigid polyurethane (PU) foam having similar density to the CNF/XG/MTM foams was also tested by flammability and cone calorimetry and is used for comparison.

The foams showed nearly instantaneous self-extinguishing behavior directly after removal of the igniting blue methane flame (Video S1, Supporting Information). Flame propagation is prevented, and the foam is virtually undamaged (final residue 93%). Only the portion of the sample exposed to the flame shows blackening as a consequence of extensive CNF charring. In contrast, a commercially available rigid PU foam show flaming combustion with vigorous flames and release of dense smoke. The LOI testing measures the minimum oxygen concentration which can sustain the combustion of the specimen. It is expressed as vol%, and the experiment is carried out in a controlled nitrogen/oxygen gas mixture. This parameter is used to rate the fire safety of a material and is included in many requirements for practical applications.[37] The CNF/XG/MTM foam achieve a LOI rating of 31.6%. This is higher than 30%, which is a threshold value and well above the range for commercially available fire-retardant FR-PU foams.[38] In addition, a comparison of LOI values for fossil-based, fire-retardant FR foams with the best performance: PVC, phenolic resin and polyimide, such a comparison shows the high performance of CNF/XG/MTM foams.[39–46]

In the more fundamental cone calorimetry test, the CNF/XG/MTM foams show very low HRR values (below 100 kW m^{-2}), which is excellent performance similar to phenolic resins (among the best foams available).[2] Smoke production is also reduced to levels close to the detection limit of the instrument. In contrast, typical values for commercial foams range from 200 to 400 m^2 m^{-2}, which is up to 30 times higher. The residue collected at the end of the test maintains the original shape of the foam. Some mechanical properties are preserved, as the material is capable of withstanding a pressure of roughly 2 kPa (Figure S1a, Supporting Information). FESEM observations of the residue showed nearly intact microscopic structure. High magnification micrographs show a reduction in the cell wall thickness, although the brick and mortar structure is still there (Figure S1b, Supporting Information). Raman spectroscopy was further employed to characterize the residue collected after combustion (Figure S3, Supporting Information). The collected spectrum clearly shows the characteristic signals produced by cellulose pyrolysis.[50] This provides preliminary information suggesting a certain graphitization degree of the char produced. Indeed, the presence of a band centered at 1596 cm^{-1} can be related to graphitic structure whereas a generally broad band (1416 cm^{-1}), resulting from the

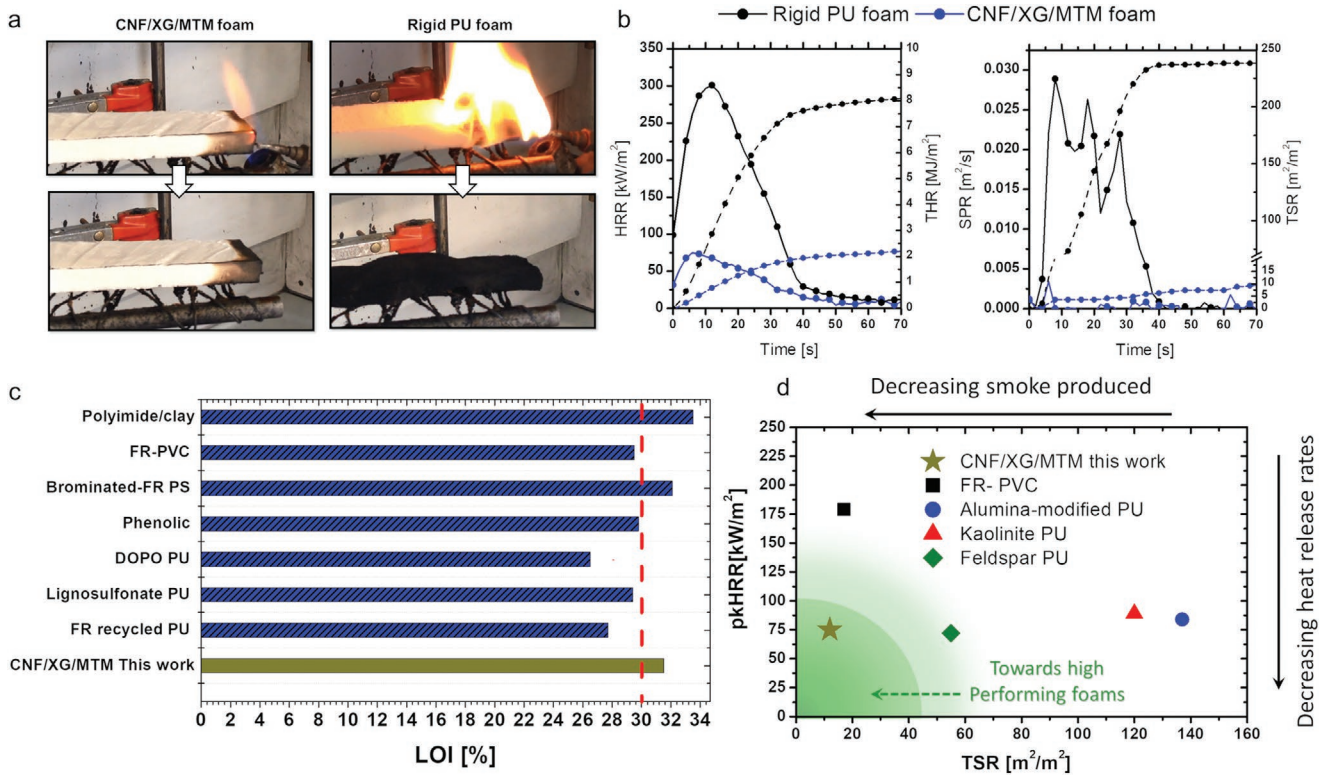

Figure 3. Flame retardant characterization: a) snapshots of the foams during horizontal flammability tests, b) cone calorimetry plots for heat and smoke release rates HRR and SPR (solid lines) and integral parameters total heat release rate THR and total smoke release TSR (dotted line), c) LOI values of tested foams in comparison with the literature, and d) comparison of cone calorimetry data (peak heat release rate) pkHRR and (total smoke release) TSR with literature data. The foam porosity is 98.5% and the composition is CNF/XG/MTM 40/27/33 wt%.

contribution of various peaks, suggests disordered amorphous carbon.[51] A comparison with pkHRR and TSR values of other foams reported in the literature (Figure 3d) further demonstrate that the FR performance of the CG/CNF/MTM foams are in the region of low pkHRR and TSR.[39,49] The low TSR values are very significant and important. Indeed, smoke plays a key role during the evacuation of a building. It affects people trying to escape the building, since smoke results in reduced ability to react, contributes to loss of consciousness, slower walking speed and long-term health effects.[50,51] For this reason smoke is often considered one of the main causes for fire fatalities.[52]

2.3. Resistance to Flame Penetration

The foam resistance to fire was tested by a lab-scale flame penetration test. It mimics the set-up of standards for larger scale evaluation of composites for aerospace applications.[53,54] The surface of a square sample is positioned in a ceramic frame and exposed to a butane/propane flame torch ($T_{flame} \approx 1300$ °C, 150 W) positioned at a fixed distance. The ability to maintain the structural integrity and provide thermal insulation to the unexposed side is evaluated. Three thermocouples are positioned at the front, middle and back of the specimen, to evaluate the temperature change during the test and calculate through-thickness temperature drops. It is uncommon to test polymer foams in these conditions, since fossil-based foams have such poor performance that they are not even considered for this test. **Figure 4** shows the set-up, snapshot images of the foam during the tests and the average temperature profiles.

The CNF/XG/MTM foams are capable of withstanding flame penetration of the torch while maintaining the structural integrity (Figure 4a). Indeed, no changes in shape or size of the specimen are detected during the test; the foam maintains its integrity, successfully preventing flame penetration and resulting in a temperature plateau at about 120 °C on the unexposed side of the foam. It means the through-thickness temperature drop is equivalent to a thermal gradient of about 680 °C cm^{-1}. During the initial 60 s, a temperature peak is observed at the center (through-thickness) (500 °C) and back side of the foam (150 °C); this can be ascribed to the decomposition of both the CNF and XG polymeric phases. Indeed, from thermogravimetric analysis (TGA), these components are known to start degradation in the 280–360 °C range. It is first characterized by an endothermic step followed by an exothermic one that leads to the formation of a thermally stable charred structures.[55,56] The residues collected after the test were investigated by FESEM and IR spectroscopy in ATR configuration (**Figure 5**).

FESEM micrographs clearly show that the internal cell structure of the foams was largely preserved. On the other hand, the cell wall thickness was reduced due to the decomposition processes of CNF and XG, where thermally stable and compact structures were formed. This is in agreement with previously reported morphological investigations of

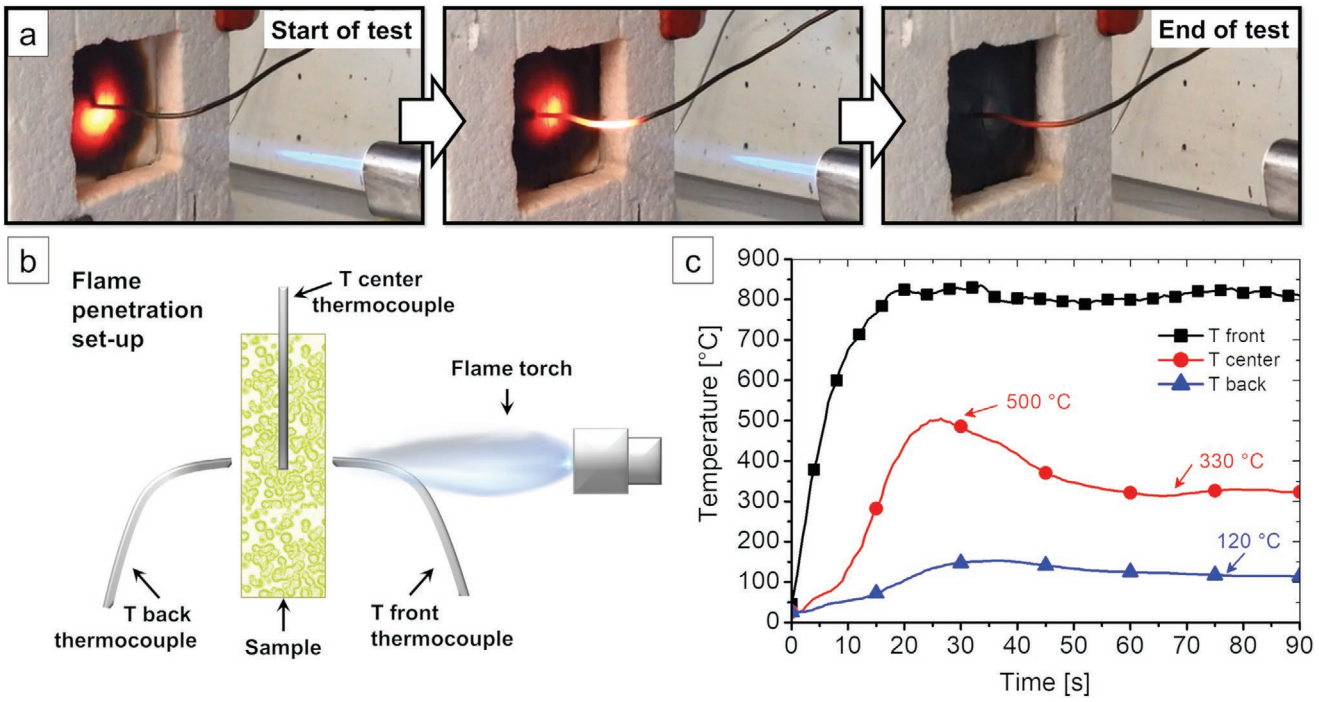

Figure 4. Flame penetration test: a) snapshot of the test of CNF/XG/MTM foam with 98.5% porosity, b) sketch of the set-up and positioning of thermocouples, and c) average temperature profiles recorded.

CNF-containing thin films before and after thermal decomposition.[57] For the residue closest to the flame, the charred structure is further oxidized in the 550–600 °C range. In the bulk of the foam, the relatively low temperature and absence of oxygen favours thermal decomposition without oxidation. This interpretation is supported by infrared spectroscopy performed at various positions through the thickness, see Figure 5. The first layer, close to the impinging flame, is almost exclusively

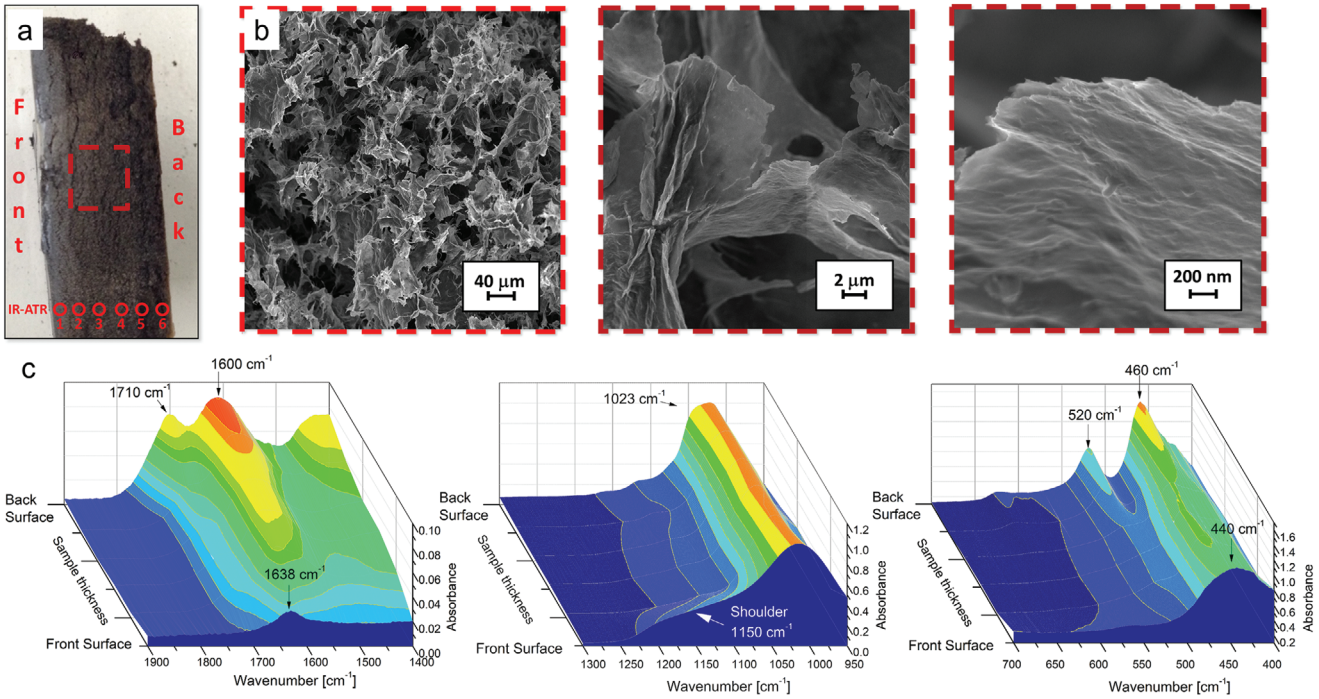

Figure 5. Post-test residue analyses: a) digital images of the CNF/XG/MTM foam, b) FESEM observation of the core of the foams at different magnifications, and c) IR surface profiles resulting from IR-ATR spectra recorded at different positions on the foam cross-section.

composed of inorganics. In this layer, the IR spectrum of MTM is changed by a broadening of the Si—O stretching signal (centered at 1023 cm^{-1}) and the merge of Al—O—Si and Si—O—Si deformation signals at 520 and 460 cm^{-1}, respectively.[58] Such changes are ascribed to structural changes in MTM due to the high temperatures.[59,60] The foam residue composition changes by further away from the flame. MTM signals switch back to "normal," showing that the temperature was not high enough to change the structure. The peak at 1600 cm^{-1} suggest the formation of an aromatic residue.[61] The peak height increases towards the unexposed surface. This is in support of a thermally stable char preserving the foam structure, and preventing flame penetration. On the back surface, the C=O group (1710 cm^{-1}) suggests limited thermal oxidation of the foam, due to the air environment and relatively high temperatures. Based on the performed characterization and residue analysis it is possible to briefly discuss a likely flame retardant mechanism for these foams. Upon exposure to a flame or a heat flux, the porous structure of the foam produces low heating rates that subsequently favor the cellulose char production from the bulk.[62] The presence of MTM helps in maintaining the original foam structures producing a mechanically stable residue where clay nanoplates are embedded within a thermally stable char.[30] By this way a limited amount of combustible volatiles is released producing the observed self-extinguishing behavior and very low HRR and SPR values. In addition, during flame penetration tests, the presence of MTM further limits the solid state char oxidation by limiting oxygen diffusion within the foam structure.[63] The collected results demonstrate excellent flame shielding properties of CNF/XG/MTM foams. Potential applications include building materials, lightweight foam cores and fire-safe materials in ground or aerospace transportation.

3. Conclusions

Green, lightweight and flame-retardant foams of 98.5% porosity were prepared based on nanocellulose and montmorillonite. Xyloglucan, a native, high-molar mass polysaccharide available as a food waste product in the form of tamarind seeds, is used as a binder improving the interaction between CNF and clay. The response to a direct flame was characterized by horizontal flame test and limiting oxygen index. The foams exhibited self-extinguishing behaviour and LOI values above 30%, which is a safe threshold for many practical applications. Cone calorimetry tests showed extremely low heat release and smoke production rates. A comparison with the literature demonstrated that the flame retardant properties of the foams are equal or superior to most of the high performance foams based on fossil-based polymers such as polyimide and phenolic foams. The resistance to fire was also evaluated by exposing the foams to a flame torch in a lab-scale flame penetration test. Despite the high organic content (67 wt%), the CNF/XG/MTM foams could withstand penetration of the flame and the high surface temperature reached during the test, which averaged 800 °C. By maintaining structural integrity and porosity, the foam successfully insulated the unexposed side, leading to impressive temperature drops (≈680 °C cm^{-1}).

For self-extinguishing properties, the 33 wt% of clay nanoplatelets have a critical role in the CNF/XG/MTM cell wall nanocomposite, by acting as a barrier which delays the release of organic volatiles to feed the flame and hinders oxygen diffusion, which would otherwise facilitate combustion. In the flame torch/flame penetration test, the MTM closest to the flame forms a high porosity ceramic structure by fusion of the MTM nanoplatelets. This structure is thermally stable, with very low thermal diffusivity, which explains the large temperature drop. In conclusion, these results pave the way for insulating materials based on renewable resources, which combine sustainability with fire protection properties.

4. Experimental Section

Materials: The xyloglucan solution was prepared from industrially available xyloglucan powder extracted from tamarind seed (weight average molecular mass 2.0 MDa, Innovasynth Technologie Ltd., India). In order to obtain xyloglucan of higher purity, the xyloglucan powder was first diluted in 0.5% Milli-Q water solution, centrifuged at 4000 rpm for 45 min and freeze-dried. The CNF suspension was obtained by enzymatic pretreatment of a sulfite pulp (Nordic AB, Sweden), as described elsewhere.[64]

The clay suspension (Cloisite Na^+, 2.86 g cm^{-3}, BYK Additives, Germany) was prepared by distributing 0.5 wt% powder in Milli-Q water using an Ultra-Turrax shear mixer equipment at 15 000 rpm for 30 min, followed by sonication at 50 W for 5 min. The suspension was then centrifuged at 4500 rpm for 30 min. The supernatant fraction was kept, and sediment was discarded. The sonication/centrifugation process was repeated until there was no visible sediment fraction, typically three times. The final concentration of the clay suspension was 0.25–0.35 wt%.

Foam Preparation: The foams were prepared by freeze-drying of colloidal suspension. First, the XG was adsorbed onto clay platelets. The MTM/XG weight ratio of the suspension was 55/45. Then, the MTM/XG suspension was mixed with 40% CNF (Table S1, Supporting Information). The ternary MTM/XG/CNF mixture was then concentrated using a roto-evaporator. The gel-like suspension was then poured in a 13.5 cm diameter polystyrene dish, with about 1 cm in thickness. It was cooled overnight at 4 °C, and subjected to freezing in liquid nitrogen from the bottom and from the sides. During this step, pure ice crystals were formed, and the particles were pushed into interstitial regions. The ice was then sublimated at low-pressure (<0.1 hPa) and ambient temperature (ScanVac Labconco, Denmark), leaving a highly porous template (98.5%) termed a "foam." Sample composition, density and relative density are detailed in Table S1 in the Supporting Information.

Characterization: The morphology of prepared materials and postcombustion residues was evaluated by Field Emission Scanning Electron Microscopy (FESEM, Zeiss Merlin 4248, beam voltage: 5 kV). The foams were cut into small pieces (approx. 10 × 10 × 10 mm^3) and pinned up on conductive adhesive tapes and chromium coated prior to FESEM observations. Energy-dispersive X-ray spectroscopy analyses were performed on a Scanning Electron Microscope (SEM, Zeiss EVO 15 equipped with a ULTIM MAX 40 probe) on a gold coated cross-section of the foam. The compression tests were performed in a Universal Materials Testing Machine (Instron 5944, USA) equipped with a 500 N load cell. The compression strain rate was set to 10% min^{-1}. The modulus was calculated as the highest slope average from the initial linear region of the stress–strain curves. The yield stress was determined as the stress at the intersection between the line tangent to the elastic region and the tangent line of the collapse region. At least four specimens were tested and the reported values in Table S2 in the Supporting Information are average data.

Flammability tests were performed in horizontal configuration by applying a 20 mm blue methane flame on the short side of specimen ($30 \times 100 \times 10$ mm^3) positioned on a metallic grid, accordingly with ASTM D 4986 standard. The flame was firstly applied for 3 s; when self-extinguishment occurred a second flame application of 6 s was performed. The test was repeated 3 times on each foam formulation. The final residue was calculated by weighting the sample before and after the test. LOI (Limiting Oxygen Index) tests were carried out on a FIRE oxygen index apparatus according to ASTM D2863 standard. Cone calorimetry (Fire Testing Technology,) was employed to investigate the combustion behaviour of $50 \times 50 \times 15$ mm^3 specimens under 35 kW m^{-2} radiative heat flux. Measurements were performed four times for each formulation evaluating Time to Ignition (TTI), peak of Heat Release Rate (avHRR and pkHRR), Total Heat Release (THR), Total smoke release (TSR) and final residue. Average values are presented with their experimental deviations. Prior to flammability and cone calorimetry tests, all specimens were conditioned at 23 ± 1 °C for 48 h at 50% R.H. in a climatic chamber. Flame penetration tests were performed on square specimens ($50 \times 50 \times 10$ mm^3) positioned in a ceramic frame, held in vertical position.[63,65] During the test, a 150 W flame generated from a butane flame torch positioned 100 mm from the surface of the specimen was focused on its centre. The torch was applied continuously for 3 min. Three thermocouples (stainless steel sheathed K-type; 1 mm diameter) were used to monitor the temperature profile on the surface exposed to the flame (T_{front}), the middle portion of the specimen (T_{middle}) and the unexposed back side (T_{back}). The test was duplicated for each different formulation. Fourier transformed-infrared in attenuated total reflectance (FT-IR ATR) was used to analyze postcombustion residues. Spectra were collected in the range 4000–700 cm^{-1} (16 scans and 4 cm^{-1} resolution) at room temperature using a spectrometer (Perkin Elmer mod. Frontier, Waltham, MA, USA) equipped with a germanium crystal. Raman spectra were collected with an In Via Raman (Renishaw) equipped with a argon laser (514 nm/50 mW, 10 scans) coupled with a Leica DM 2500 optical microscope.

Supporting Information

Supporting Information is available from the Wiley Online Library or from the author.

Acknowledgements

The authors want to thank Mauro Raimondo for FESEM analyses. In addition, the authors would like to acknowledge the FireFoam project funded by SSF (RMA11-0065) in Sweden.

Conflict of Interest

The authors declare no conflict of interest.

Author Contributions

F.C., J.K., and L.A.B. conceived the experiments. F.C. and L.A.B. coordinated the project. F.C. and L.M. performed the characterization and data elaboration. F.C., L.M., and L.A.B. contributed to the discussion and interpretation of the results. The manuscript was mainly written by F.C. and L.A.B.

Data Availability Statement

Research data are not shared.

Keywords

flame retardancy, foams, montmorillonite, nanocellulose, xyloglucan

Received: June 30, 2021
Revised: July 30, 2021
Published online: August 31, 2021

[1] M. Ahrens, *Home Fires That Began with Upholstered Furniture*, National Fire Protection Association Quincy, MA, USA **2008**.
[2] J. P. Hidalgo, J. L. Torero, S. Welch, *Fire Mater.* **2018**, *42*, 358.
[3] H. M. Stapleton, S. Klosterhaus, A. Keller, P. L. Ferguson, S. van Bergen, E. Cooper, T. F. Webster, A. Blum, *Environ. Sci. Technol.* **2011**, *45*, 5323.
[4] G. Stieger, M. Scheringer, C. A. Ng, K. Hungerbuhler, *Chemosphere* **2014**, *116*, 118.
[5] J. H. Troitzsch, *J. Fire Sci.* **2016**, *34*, 171.
[6] S. Qiu, Y. Zhou, X. Zhou, T. Zhang, C. Wang, R. K. Yuen, W. Hu, Y. Hu, *Small* **2019**, *15*, 1805175.
[7] S. Qiu, C. Ma, X. Wang, X. Zhou, X. Feng, R. K. Yuen, Y. Hu, *J. Hazard. Mater.* **2018**, *344*, 839.
[8] S. Qiu, X. Wang, B. Yu, X. Feng, X. Mu, R. K. Yuen, Y. Hu, *J. Hazard. Mater.* **2017**, *325*, 327.
[9] S. Qiu, W. Xing, X. Feng, B. Yu, X. Mu, R. K. Yuen, Y. Hu, *Chem. Eng. J.* **2017**, *309*, 802.
[10] G. Malucelli, F. Bosco, J. Alongi, F. Carosio, A. Di Blasio, C. Mollea, F. Cuttica, A. Casale, *RSC Adv.* **2014**, *4*, 46024.
[11] H. Yang, B. Yu, X. Xu, S. Bourbigot, H. Wang, P. Song, *Green Chem.* **2020**, *22*, 2129.
[12] M. Kardung, K. Cingiz, O. Costenoble, R. Delahaye, W. Heijman, M. Lovrić, M. van Leeuwen, R. M'Barek, H. van Meijl, S. Piotrowski, *Sustainability* **2021**, *13*, 413.
[13] J. Alongi, F. Cuttica, F. Carosio, *ACS Sustainable Chem. Eng.* **2016**, *4*, 3544.
[14] R. Davis, Y. C. Li, M. Gervasio, J. Luu, Y. S. Kim, *ACS Appl. Mater. Interfaces* **2015**, *7*, 6082.
[15] D. Battegazzore, A. Frache, F. Carosio, *Composites, Part B* **2020**, *200*, 108310.
[16] L. Maddalena, J. Gomez, A. Fina, F. Carosio, *Nanomaterials* **2021**, *11*, 266.
[17] L. Maddalena, F. Carosio, J. Gomez, G. Saracco, A. Fina, *Polym. Degrad. Stab.* **2018**, *152*, 1.
[18] *Multilayer Thin Films: Sequential Assembly of Nanocomposite Materials*, 2nd ed. (Eds: D. Gecher, J. B. Schlenoff), Wiley-VCH, Weinheim, Germany **2012**.
[19] K. M. Holder, R. J. Smith, J. C. Grunlan, *J. Mater. Sci.* **2017**, *52*, 12923.
[20] O. Koklukaya, F. Carosio, L. Wågberg, *ACS Appl. Mater. Interfaces* **2017**, *9*, 29082.
[21] M. Ghanadpour, B. Wicklein, F. Carosio, L. Wågberg, *Nanoscale* **2018**, *10*, 4085.
[22] H.-B. Chen, D. A. Schiraldi, *Polym. Rev.* **2018**, *59*, 1.
[23] Y.-T. Wang, H.-B. Zhao, K. Degracia, L.-X. Han, H. Sun, M. Sun, Y.-Z. Wang, D. A. Schiraldi, *ACS Appl. Mater. Interfaces* **2017**, *9*, 42258.
[24] K. Shang, J.-C. Yang, Z.-J. Cao, W. Liao, Y.-Z. Wang, D. A. Schiraldi, *ACS Appl. Mater. Interfaces* **2017**, *9*, 22985.
[25] H. Sun, D. A. Schiraldi, D. Chen, D. Wang, M. Sánchez-Soto, *ACS Appl. Mater. Interfaces* **2016**, *8*, 13051.
[26] D. Klemm, F. Kramer, S. Moritz, T. Lindstrom, M. Ankerfors, D. Gray, A. Dorris, *Angew. Chem.* **2011**, *50*, 5438.
[27] A. E. Donius, A. Liu, L. A. Berglund, U. G. Wegst, *J. Mech. Behav. Biomed. Mater.* **2014**, *37*, 88.

[28] A. Liu, L. Medina, L. A. Berglund, *ACS Appl. Mater. Interfaces* **2017**, *9*, 6453.
[29] L. Medina, F. Carosio, L. A. Berglund, *Compos. Sci. Technol.* **2019**, *182*, 107762.
[30] F. Carosio, J. Kochumalayil, F. Cuttica, G. Camino, L. Berglund, *ACS Appl. Mater. Interfaces* **2015**, *7*, 5847.
[31] J. Kochumalayil, H. Sehaqui, Q. Zhou, L. A. Berglund, *J. Mater. Chem.* **2010**, *20*, 4321.
[32] T. Hayashi, *Annu. Rev. Plant Biol.* **1989**, *40*, 139.
[33] N. C. Carpita, D. M. Gibeaut, *Plant J.* **1993**, *3*, 1.
[34] Y. Wang, J. Wohlert, M. Bergenstråhle-Wohlert, J. J. Kochumalayil, L. A. Berglund, Y. Tu, H. Ågren, *Biomacromolecules* **2014**, *16*, 257.
[35] J. J. Kochumalayil, S. Morimune, T. Nishino, O. Ikkala, A. Walther, L. A. Berglund, *Biomacromolecules* **2013**, *14*, 3842.
[36] B. Schartel, T. R. Hull, *Fire Mater.* **2007**, *31*, 327.
[37] M. Suzanne, M. Delichatsios, J. Zhang, *Combust. Flame* **2014**, *161*, 288.
[38] H. Singh, A. Jain, *J. Appl. Polym. Sci.* **2009**, *111*, 539.
[39] Z. Wang, Z. Huang, X. Li, J.-a. Zhou, *Composites, Part A* **2019**, *121*, 180.
[40] Y. Wang, H. Jiang, J. Ni, J. Chen, H. Zhou, X. Wang, F. Xin, *RSC Adv.* **2019**, *9*, 192.
[41] P. Xu, Y. Yu, M. Chang, J. Chang, *Polymers* **2019**, *11*, 1471.
[42] J. F. Qiu, M. Q. Zhang, M. Z. Rong, S. P. Wu, J. Karger-Kocsis, *J. Mater. Chem. A* **2013**, *1*, 2533.
[43] W. Lu, Q. Li, Y. Zhang, H. Yu, S. Hirose, H. Hatakeyama, Y. Matsumoto, Z. Jin, *J. Wood Sci.* **2018**, *64*, 287.
[44] M. Li, J. Luo, Y. Huang, X. Li, T. Yu, M. Ge, *J. Appl. Polym. Sci.* **2014**, *131*, 40857.
[45] C. Wang, Y. Wu, Y. Li, Q. Shao, X. Yan, C. Han, Z. Wang, Z. Liu, Z. Guo, *Polym. Adv. Technol.* **2018**, *29*, 668.
[46] L. Yan, L. Fu, Y. Chen, H. Tian, A. Xiang, A. V. Rajulu, *J. Appl. Polym. Sci.* **2017**, *134*, 44828.
[47] M. W. Smith, B. Pecha, G. Helms, L. Scudiero, M. Garcia-Perez, *Biomass Bioenergy* **2017**, *104*, 17.
[48] M. W. Smith, I. Dallmeyer, T. J. Johnson, C. S. Brauer, J.-S. McEwen, J. F. Espinal, M. Garcia-Perez, *Carbon* **2016**, *100*, 678.
[49] A. Agrawal, R. Kaur, R. S. Walia, *Fire Mater.* **2019**, *43*, 917.
[50] H. Frantzich, *A Model for Performance-Based Design of Escape Routes*, Department of Fire Engineering, Lund Institute of Technology, Lund University, **1994**.
[51] R. G. Gann, *Fire Technol.* **2004**, *40*, 201.
[52] J. Giebułtowicz, M. Rużycka, P. Wroczyński, D. A. Purser, A. A. Stec, *Forensic Sci. Int.* **2017**, *277*, 77.
[53] P. Tranchard, F. Samyn, S. Duquesne, M. Thomas, B. Estèbe, J.-L. Montès, S. Bourbigot, *J. Fire Sci.* **2015**, *33*, 247.
[54] J. Bartlett, C. Stratford, *Practical Failure Analysis* **2001**, pp. 37–43, https://doi.org/10.1007/BF02715378.
[55] M. Ramiah, *J. Appl. Polym. Sci.* **1970**, *14*, 1323.
[56] D. Davies, A. Horrocks, M. Greenhalgh, *Thermochim. Acta* **1983**, *63*, 351.
[57] F. Carosio, M. Ghanadpour, J. Alongi, L. Wågberg, *Carbohydr. Polym.* **2018**, *202*, 479.
[58] Z. Navratilova, P. Wojtowicz, L. Vaculikova, V. Sugarkova, *Acta Geodyn. Geomater.* **2007**, *4*, 59.
[59] P. Wu, H. Wu, R. Li, *Spectrochim. Acta, Part A* **2005**, *61*, 3020.
[60] C. Volzone, L. Garrido, *Procedia Mater. Sci.* **2012**, *1*, 164.
[61] S. Soares, G. Camino, S. Levchik, *Polym. Degrad. Stab.* **1995**, *49*, 275.
[62] J. Alongi, G. Camino, G. Malucelli, *Carbohydr. Polym.* **2013**, *92*, 1327.
[63] F. Carosio, J. Kochumalayil, A. Fina, L. A. Berglund, *Adv. Mater. Interfaces* **2016**, *3*, 1600551.
[64] M. Henriksson, G. Henriksson, L. Berglund, T. Lindström, *Eur. Polym. J.* **2007**, *43*, 3434.
[65] F. Carosio, L. Maddalena, J. Gomez, G. Saracco, A. Fina, *Adv. Mater. Interfaces* **2018**, *5*, 1801288.